Simulation of the growth of metal nanoclusters on the MgO(100) surface

Jacek Goniakowski[1,2] and Christine Mottet[3]
[1]*CNRS, Institut des Nanosciences de Paris, UMR 7588, 140 rue de Lourmel, 75015 Paris, France*
[2]*UPMC–Université Paris 06, INSP, UMR 7588, 140 rue de Lourmel, 75015 Paris, France*
[3]*CINaM, CNRS, Campus de Luminy, Case 913, 13288 Marseille Cedex 9, France*
(Received 8 February 2010; revised manuscript received 26 March 2010; published 20 April 2010)

The growth of Pd, Pt, and Ag clusters on the MgO(001) substrate is simulated with the aim to determine particle shape and structural characteristics in relation with data issued from atom-by-atom growth experiments in UHV conditions. Metal-metal interactions are modeled by a second-moment approximation tight-binding potential, while metal-oxide interactions are modeled by an analytic function fitted to first-principles calculations. The cluster growth is simulated with molecular dynamics and followed up to a cluster size of 400 atoms. We show that while at typical experimental temperatures the smallest clusters are melted, the attachment of subsequent adatoms leads to cluster crystallization. Upon crystallization the particles adopt the low-energy structure corresponding to the crystallization size. This latter determines to a large extent the final form of large clusters issued from atom-by-atom growth. Within such a scenario, experimentally observed larger Pd and Pt particles in (001) epitaxy with the substrate may result from kinetic blocking, while the equilibrium shape of large clusters, with metal (111) facet in contact with the oxide substrate, may be unreachable at typical experimental temperatures.

DOI: 10.1103/PhysRevB.81.155443 PACS number(s): 68.47.Jn, 68.55.A−, 61.46.Df, 68.35.−p

I. INTRODUCTION

Metal clusters supported on oxide surfaces have been a subject of considerable attention due to their possible applications in most various fields ranging from heterogeneous catalysis to electronics and magnetic devices.[1] The applicative context has largely motivated also more fundamental studies on model systems obtained by a controlled metal deposition on a well characterized oxide surface in UHV conditions.[2,3] With the goal to identify the principal factors responsible for particle properties, these studies required an adequate characterization of their structural characteristics and, in particular, of the substrate-induced features. Since the type, density, and spatial distribution of undercoordinated sites are expected to give the principal contribution to the characteristics of metal nanoclusters, a special attention was given to a detailed characterization of particle shape and morphology as a function of their size.

Nowadays, complementary information concerning particle shape, structure, and morphology can be systematically obtained by looking either at individual particles in high-resolution transmission electron microscopy (Ref. 4) and near field (scanning tunneling or atomic force microscopy) experiments,[5] or by *in situ* observation of collections of clusters by grazing-incidence small-angle x-ray scattering (GISAXS).[6–9] Moreover, this latter approach has been used to follow particle growth and to determine the relationship between clusters' structural properties and their growth conditions. For example, *in situ* growth of Ag (Refs. 6 and 7) and Pd (Refs. 8 and 9) by physical evaporation on the MgO(100) surface leads principally to face-centered-cubic (fcc) particles in a truncated cubo-octahedral shape and in the so-called cube-on-cube $(001)_{\mathrm{Metal}}\|(001)_{\mathrm{MgO}}$ epitaxy relationship with the substrate. In the following, we will refer to such clusters as in (100) epitaxy or fcc(100) ones. The difference between their lateral and vertical size distribution is believed to originate from the growth mechanism.[7,9] For both these metals a small fraction of fcc particles in a truncated cubo-octahedral shape and in $(111)_{\mathrm{Metal}}\|(001)_{\mathrm{MgO}}$ interfacial orientation was also observed.[6,10,11] We will refer to these latter as in (111) epitaxy or fcc(111) ones. Conversely, in the case of Pt it has been found that the (111) and (100) epitaxies coexist at low temperature and that the (100) one tends to dominate only in particles obtained at higher temperatures.[12]

We have recently performed a systematic theoretical analysis of the behavior of the equilibrium shape as a function of size for Ag, Pd, and Pt clusters on the MgO(100) surface at 0 K.[13,14] We have found that for all metals, the preferred structures of small clusters is in fcc(100) cube-on-cube epitaxy with the substrate. Depending on the metal, clusters in the (111) epitaxy may be favored at larger clusters. For example, Ag clusters tend to preserve the (100) epitaxy in all considered size ranges (up to about 3000 atoms), while the transition to the (111) epitaxy occurs at about 500 and 200 atoms, respectively, for Pt and Pd particles. While in the case of Au and Ag the computational results agree fairly well with the experimental evidence, such comparison is much less straightforward for Pd and Pt, where a possible effect of temperature on the shape of observed particles has been evoked. This latter has been analyzed in our subsequent systematic study on recrystallization of Ag, Pd, and Pt nanoclusters on the MgO(001) surface.[15] It showed that the cluster structural and morphological aspects are little influenced by the temperature, so that the most stable 0 K structures can be considered as a good approximation of the finite-temperature ones. Only in the case of Pt, where the structures in fcc(100) and fcc(111) epitaxies are quasidegenerate over a relatively large range of cluster sizes, the temperature effects may enhance the stability of the (100) epitaxy to sizes somewhat larger than expected at 0 K.

However, we need to keep in mind that growth conditions may influence the particle shape. Indeed, the increase in temperature in growth experiments enhances not only the ada-

tom diffusion on each particle, but also the adatoms and cluster diffusion on the oxide substrate. This leads to Ostwald ripening which impedes an efficient stabilization of small metal nanoparticles. As a consequence, experimental nanoclusters are systematically produced in a quite narrow range of thermal treatment, and the question is to what extent these growth conditions influence their shape and structural characteristics? In this context, the goal of the present study is to investigate the shape of particles obtained in the UHV conditions in atom-by-atom growth experiments. We will show that the smallest clusters are fully or partially melted at typical temperatures used in experiments. The attachment of subsequent adatoms leads to cluster crystallization upon which particles adopt the low-energy structure at the crystallization size. This low-energy structure determines to a large extent the final form of large clusters issued from atom-by-atom growth. Within such a scenario, the larger fcc(100) Pd and Pt particles observed in growth experiments may result from kinetic blocking due to an insufficiently high temperature. Our results suggest that the fcc(111) equilibrium shape of large clusters may be unreachable at typical experimental temperatures.

The paper is structured as follows. Section II contains the description of the model of interactions, of growth simulations method, and of tools used to analyze the results. In Sec. III, we detail the results obtained for Ag, Pd, and Pt clusters with a special emphasis on the case of Pt. We relate them to the data issued from 0 K optimization and from recrystallization simulations. We end by a synthetic comparative presentation of results on the three considered metals Ag, Pd, and Pt and a discussion in the context of available experimental evidence in Sec. IV.

II. METHODOLOGY

All growth simulations reported in this paper are performed with a constant-temperature molecular-dynamics (MD) approach. Starting from a small (seed) particle, metal adatoms are added one by one at fixed time intervals, slowly enough to enable cluster equilibration between the subsequent additions. To enable simulations of an adequate length we employ a semiempirical energetic model based on the second-moment approximation in the tight-binding scheme for the metal-metal interaction, complemented by a many-body potential energy surface (PES) fitted to results of *ab initio* calculations for the metal-oxide interactions.

A. Model of interactions

Following Ref. 16, we write the binding energy of a supported metal cluster as the sum of atomic contributions due to metal-metal and to metal-oxide interactions. The functional form of the metal-metal potential is derived within the second-moment approximation to the tight-binding model (TB-SMA potential),[17–19] with the parameters fitted to experimental bulk quantities. Full details on this implementation of the TB-SMA potential, together with the particular set of parameters for Pt, Pd, and Ag, are given in Refs. 20–22. This approach has been already used in the study on structural transitions in icosahedral, decahedral, and octahedral free metal nanoclusters,[20,22] and its validation against existing density-functional theory (DFT) results on metal nanoclusters has been discussed.[23,24] We remind that while this parametrization of the TB-SMA results in a systematic underestimation of the surface energies, the anisotropy factor (001)/(111) is being reproduced fairly well.

The functional form of the effective metal-MgO interaction was constructed and parametrized as described in our earlier works on Pd/MgO(001),[14,16] Ag/MgO(001),[13,25] and Pt/MgO(001).[12,14] The interaction was assumed additive with respect to metal atoms but explicitly dependent on their coordination. Such a (nonlinear) dependence of the interaction energy on the metal coordination is particularly important in systems with a large proportion of undercoordinated atoms (small clusters) and confers to the fitted PES an effective many-body character. In the case of Pd and Pt, the analytical form of the interaction was adjusted to the results of DFT calculations performed on a series of model systems including three different high symmetry metal adsorption sites (oxygen, magnesium, and hollow) and three different metal coverages (0.25, 1.0, and 2.0 or 5.0 ML).[12,16] In the case of Ag, as to account correctly for the enhancement of adhesion energy due to the stabilizing contribution of metal atoms above the one directly interacting with the substrate,[26] a five-atom square pyramid was used instead of the monolayer. The corresponding sets of parameters are listed in Ref. 27. We stress that in all DFT calculations the metal/oxide systems were thoroughly relaxed. As a consequence, the present PES approach neglects only the differential relaxation of the MgO(100) surface, i.e., the difference between MgO(100) relaxation at model metal/MgO(100) interfaces used in DFT calculations and that at an actual cluster/MgO(100) interface.

B. Finite temperature and growth simulations

The above interaction model has already been used for finite temperature simulations of supported metal nanoclusters in canonical molecular-dynamics studies of cluster fusion and recrystallization.[15,28,29] In such simulations the temperature is maintained by an Andersen thermostat,[30] which couples the cluster to a heat bath (here the MgO substrate). The bath causes stochastic collisions generating a Maxwell-Boltzmann distribution of the velocities. Between two stochastic collisions, the system evolves according to the classical Newton's equations, which are numerically solved by the velocity Verlet algorithm.[31] We have checked that this simple method is almost equivalent to the more elaborated approximation called the surface oscillator model,[32] where the motion of substrate atoms is taken explicitly into account, but approximated by a single three-dimensional harmonic oscillator.

As to avoid the time-consuming stage of metal adatoms diffusion over the MgO(100) surface, in all growth simulations the subsequent adatoms are (randomly) placed directly at the oxide-metal-vacuum triple line. Such an approach accounts for adatoms arriving by diffusion over the MgO(100) surface and neglects those landing directly on the metal cluster. It is thus particularly adequate for the simulation of early

growth stages (small clusters). The time interval between the arrivals of subsequent adatoms was fixed to about 7 ns (a million of MD steps). It is of the order of a typical time interval between two collisions between a free cluster and adatoms in a vapor pressure of $P=3$ mbar.[33] The experimental flux f can be expressed as

$$f = \frac{4\pi r^2 P}{\sqrt{2\pi mkT}} \quad (1)$$

at a temperature T, for a particle of radius r and mass m. As discussed in the context of growth simulations on unsupported metal clusters,[34] such a time interval is fully adequate for adatom equilibration on the metal particle. This interval is considerably shorter compared to typical deposition rates estimated for UHV evaporation experiments (0.001–10 s).[6,9,12]

All the simulations were initiated from a seed particle of about 30 atoms. We will see that at all considered temperatures they were fully or partially melted at the beginning of cluster growth avoiding thus a possible bias induced by this arbitrary choice.

C. Order parameters

At each stage of particle growth (for each cluster size) the behavior of cluster shape and structure was monitored by about 1000 snapshots of its instantaneous structure taken in regular intervals. The reported averages run over these instantaneous structures. The cluster shape was quantified with two parameters: the height to diameter ratio $I_\perp = 2I_z/(I_x+I_y)$ and the length to width ratio $I_\parallel = 2|I_x - I_y|/(I_x+I_y)$, where I_x and I_y are the components of the diagonalized tensor of inertia parallel to the MgO(100) surface, and I_z is the perpendicular component. The epitaxy relation with the MgO(100) substrate was monitored by the average coordination number of metal atoms in the interfacial layer Z_{int}. Finally, the local order parameters are derived from the common neighbor analysis (CNA).[35,36] The CNA signature, defined for each pair of nearest neighbors, is composed of three integer numbers (nbp) representing the number of common neighbors n, the number of bonds between shared neighbors b, and the number of bonds in the longest bond path formed among the shared neighbors p. It enables to distinguish the fcc, hcp, and fivefold symmetries [icosahedral (Ih) or decahedral (Dh)] with, respectively, the (421), (422), and (555) signatures.

III. RESULTS

We start by a detailed presentation of results on the calculated characteristics of Pt clusters focusing on the behavior of their structure and shape during particle growth at different temperatures. Then we synthetically present the results for the series of metals: Ag, Pd, and Pt, and discuss the major metal-dependent features.

A. Atom-by-atom growth of Pt clusters

In the case of MgO(100)-supported Pt clusters, we have systematically started the simulations with a 31-atom-large fcc(111) cluster and followed its growth up to a size of 400 atoms at three different temperatures: 600, 800, and 1000 K. At each temperature the results were collected over 16 independent runs.

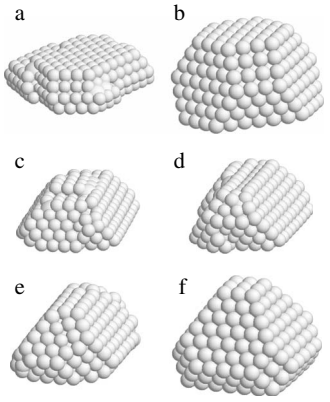

FIG. 1. Comparison of typical Pt clusters issued from atom-by-atom growth at three different temperatures [(a) and (c) 600 K; (d) 800 K; (e) 1000 K] with the corresponding ones, issued from optimization at 0 K [(b) and (f)].

1. Structural and shape characteristics

Independently of the considered temperature, all clusters issued from the growth simulations are truncated fcc octahedra. When grown at higher temperatures (800 and 1000 K) they adopt the (001) epitaxy relationship with the substrate, but at 600 K we find about 20% of fcc(111) clusters. In Fig. 1(a) and Figs. 1(c)–1(e) we show typical particles issued from growth simulations at the three different temperatures and refer them to the most stable clusters obtained from the optimization of the corresponding fcc(100) and fcc(111) motifs at 0 K [(b) and (f)].

While in all cases the grown particles display a relatively well defined set of (100) and (111) facets, they do not reproduce the closed atomic shells characteristic of the optimized particles. More importantly, their shapes differ: the grown clusters are systematically flatter and more elongated compared to the optimized ones. In Table I we quantify these effects using the length to width ratio $I_\parallel$, which accounts for cluster elongation, and the height to diameter ratio $I_\perp$, which accounts for cluster flattening. Compared to the optimized particles of the same size ($I_\parallel = 0$ and $I_\perp \sim 0.46$) the grown clusters are systematically elongated (average $I_\parallel > 0$) and flattened (average $I_\perp < 0.46$). The effect is the most pronounced at 600 K and diminishes progressively at higher

TABLE I. Calculated average shape characteristics for Pt clusters grown at the three different temperatures compared to the corresponding results on the optimized particles: $I_\parallel$ and $I_\perp$. See text for details.

$I_\parallel/I_\perp$	600 K	800 K	1000 K	Equilibrium
fcc(100), 373 atoms	1.02/0.15	0.79/0.26	0.66/0.34	0.00/0.46
fcc(111), 320 atoms	0.93/0.08			0.00/0.46

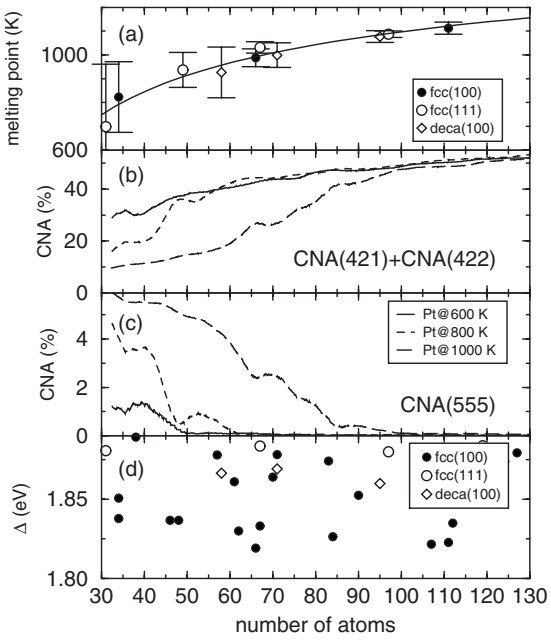

FIG. 2. (a) Calculated melting temperature T_m of MgO(100)-supported Pt clusters as a function of cluster size N. The full line represents an adjustment of a phenomenological relationship $T_m(R) \sim 1-\alpha/R$ as a function of particle radius R. [(b) and (c)] Calculated behavior of average CNA signatures as a function of cluster size for Pt clusters at MgO(100) at 600, 800, and 1000 K: (b) CNA(421)+CNA(422) (%), (c) CNA(555) (%). (d) Specific surface energy $\Delta(N)$ (eV) for the optimized fcc(100), fcc(111), and deca(100) Pt clusters as a function of particle size.

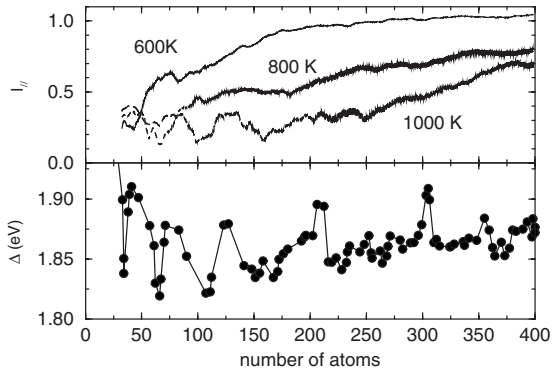

FIG. 3. (a) Behavior of the average elongation parameter $I_{\parallel}(N)$ as a function of the instantaneous cluster size N during atom-by-atom growth of Pt on the MgO(100) surface at three different temperatures: 600, 800, and 1000 K. (b) Specific surface energy $\Delta(N)$ (eV) for the optimized fcc(100) clusters as a function of cluster size N.

temperatures. However, in the considered range of growth temperatures, $I_{\parallel}$ and $I_{\perp}$ do not attain the values obtained of the optimized cluster. We also note the particularly strong flattening of the fcc(111) clusters.

2. Cluster crystallization

In order to get an insight into the changes in the crystalline structure during the growth process let us focus on the smallest particle sizes and analyze the behavior of the two principal CNA signatures: CNA(421)+CNA(422) and CNA(555), Figs. 2(b) and 2(c). We note that the local maxima of CNA(421)+CNA(422), which quantifies the proportion of local crystalline (fcc/hcp) environment, are systematically correlated with the local minima of CNA(555), corresponding to local noncrystalline/decahedral environment. As a function of cluster size this latter signature goes progressively down to zero indicating a full crystallization of the fcc structure. The corresponding crystallization size can be estimated to approximately 50, 60, and 100 atoms, respectively, for 600 K, 800 K, and 1000 K. This size-temperature relationship is consistent with the calculated behavior of the melting temperature as a function of the particle size, Fig. 2(a).

At all considered temperatures the smallest particles are fully or partially melted. During the growth the fcc structure establishes progressively, but its proportion varies as a function of cluster size. Local maxima of CNA(421)+CNA(422) and the corresponding local minima of CNA(555) at $N \sim 34$, 48, 66, and 85 atoms can be associated with the most stable optimized fcc(100) clusters deduced from the corresponding minima of specific surface energy $\Delta(N)=(E-N\epsilon_B)/N^{2/3}$ (E total cluster energy; ϵ_B the binding energy per atom in the bulk metal),[37] Fig. 2(d). Conversely, the local minima of CNA(421)+CNA(422) [maxima of CNA(555)] at $N \sim 39$, 52, 69, and 90 atoms are to be associated with the most stable optimized deca(100) clusters.

This indicates that at the crystallization stage the particles adapt their structure as to minimize the energy and follow relatively well the relative structural stability estimated by 0 K optimization. As a consequence, the most stable fcc(100) and deca(100) clusters appear in turns as the cluster size increases. However, while such changes in the cluster structure can be detected at the earliest growth stages (smallest sizes), they disappear progressively as the cluster size increases and a single (fcc) structure tends to establish.

3. Clusters in (100) epitaxy

Beyond the crystallization stage, in order to get an insight into the origin of the effect of temperature on the shape of the growing clusters, in Fig. 3(a) we plot the average elongation parameter $I_{\parallel}(N)$ as a function of the instantaneous cluster size N for the three considered growth temperatures. We focus on the fcc(100) particles which are the most abundant in all the simulations.

The results obtained for the three growth temperatures display a similar general pattern: for small cluster sizes $I_{\parallel}(N)$ goes through a sequence of well pronounced minima and maxima; for larger sizes it grows quasimonotonically before reaching a nearly constant level. The small size regime is the narrowest at 600 K (up to approximately 100 atoms) and extends progressively up to approximately 170 atoms at 800 K and up to 250 atoms at 1000 K. We note that the local minima of $I_{\parallel}(N)$, which indicate an enhanced proportion of more isotropic particles, coincide with the lowest energy optimized fcc(100) clusters ($I_{\parallel} \sim 0$), given by the minima of the specific surface energy $\Delta(N)$; Fig. 3(b). This indicates that the most stable fcc(100) particles of $N \sim 66$, 108, 140–170,

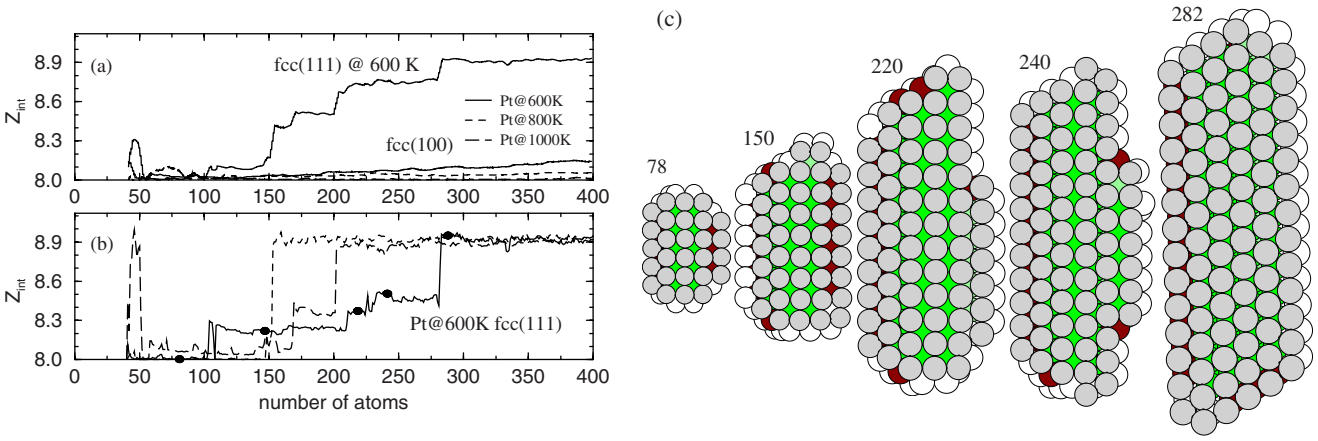

FIG. 4. (Color online) (a) Calculated behavior of the average coordination number of Pt atoms at the metal/oxide interface $Z_{int}(N)$ as a function of cluster size N for Pt clusters grown at 600, 800, and 1000 K. (b) $Z_{int}(N)$ for each of the three runs resulting in the (111) epitaxy at 600 K. Full circles represent clusters of 78, 150, 220, 240, and 282 atoms depicted in (c). (c) Snapshots of the instantaneous atomic structure of the interfacial Pt layer (gray circles) taken at different stages of particle growth.

and 215–260 atoms do indeed appear during the growth. However, while such particles can be detected at early growth stages (small size regime), larger particles adopt progressively their growth shape ($I_{\|}>0$).

4. Clusters in (111) epitaxy

At the lowest considered temperature a small fraction of clusters adopt the (111) epitaxy. To identify the origin of this epitaxy in the growth simulations, in Fig. 4 we plot the behavior of the coordination number of the interfacial Pt atoms Z_{int} as a function of the instantaneous cluster size N.

The particles found in the (111) epitaxy [$Z_{int}(N)\sim 9$] at the end of the growth simulation do systematically display a perfect (100) one at smaller sizes; Fig. 4(b). The transition between the (100) and (111) epitaxies does not occur at a unique and specific cluster size but proceeds in a sequence of steps. As exemplified in the plots of the instantaneous atomic structure of the interfacial Pt layer, Fig. 4(c), these correspond to the formation of subsequent stacking faults which transform progressively the epitaxy relation with the substrate.

On the other hand, the fcc(100) clusters systematically display $Z_{int}(N)$ values very close to that of a perfect (100) facet [$Z_{int}(N)=8$]; Fig. 4(a). Only at 600 K, Z_{int} is somewhat larger and it increases as a function of the cluster size. This effect is to be assigned to the existence of an increasing proportion of stacking faults and suggests a possibility of a slow progressive transition toward the (111) epitaxy.

We note that contrary to the cluster structure and shape described in previous subsections, the formation of subsequent stacking faults is not limited to the smallest particles only but occurs also at a relatively large cluster size and at a low growth temperature. For both thermodynamic and kinetic reasons this effect is to be ascribed to the particularly elongated and flattened cluster shape at this temperature, and, as a consequence, it is restrained to the lowest growth temperatures only.

5. Summary: Growth shape and epitaxy of Pt clusters

We find that at early stages of atom-by-atom growth the crystallizing Pt particles adopt the most energetically favorable structure coherent with the 0 K estimation. In this regime the average proportion of fcc and decahedral clusters changes rapidly as a function of particle size, as to follow changes in the relative stability of their optimized 0 K counterparts. However, the structural diversity diminishes rapidly as the particle size increases and, after full crystallization, the fcc(100) clusters dominate. While at small sizes the shape of these particles is similar to that of the optimized 0 K fcc(100) clusters, larger clusters adopt progressively an elongated and flattened shape typical for Pt particles issued from growth simulations and particularly pronounced at low growth temperatures.

Moreover, when grown at the lowest temperature, about 20% of Pt clusters transit from the fcc(100) to the fcc(111) epitaxy by a sequence of subsequent stacking faults. At this temperature, also the remaining fcc(100) particles display a non-negligible and increasing proportion of stacking faults, what suggests a possibility of a progressive slow transition to the (111) epitaxy. Conversely, at higher temperatures, the fcc(111) clusters are totally absent and the number of stacking faults in the fcc(100) particles diminishes as the growth temperature increases. Thus, the enhanced proportion of stacking faults and the related tendency toward transition between the two epitaxies are correlated with the particularly flattened and elongated shape of particles grown at the lowest temperature.

B. Trends in the series of metals: Ag, Pd, and Pt

In order to estimate the effect of the nature of metal on its growth characteristics, we have considered also the growth of Ag and Pd on the MgO(100) surface, Fig. 5. As in the case of Pt, all simulations were systematically initiated with a 31-atom-large fcc(111) cluster and its growth was followed up to the size of 400 atoms. Three different growth temperatures were systematically considered but, since the melting point of Ag (1235 K) and Pd (1828 K) are lower compared to that of Pt (2041 K), we have simulated Ag and Pd growth at 400, 600, and 800 K. Depending on the case, the statistics were collected over 6–20 independent runs.

In the case of Ag, the growth at 800 K does not result in cluster crystallization within the considered size range. If grown at the intermediate temperature (600 K), Ag clusters crystallize at about 130–140 atoms as truncated fcc octahedra in the (100) epitaxy with the substrate. Their shape and epitaxy do not change during the further growth. At the lowest considered temperature (400 K) the crystallization occurs already at about 50 atoms. At this temperature the majority of clusters adopt the (100) epitaxy, but about 30% of clusters are found in the (111) one. Contrary to the case of Pt discussed in the previous sections, these latter are formed already at the crystallization stage rather than by a sequence of stacking faults in crystallized fcc(100) clusters. They are to be related to the comparable stability of the smallest ($N < 50$) fcc(100) and fcc(111) Ag clusters.

Pd clusters crystallize as truncated fcc octahedra, at sizes between 50 and 100 atoms at lower temperatures (400 and 600 K), and at about 150 atoms at 800 K. At all temperatures Pd clusters adopt principally the (100) epitaxy but, if grown at 400 K, 20% of them transit to the (111) one. As in the case of Pt, the transition occurs by a sequence of stacking faults formed in 100–150 atoms size range. At this temperature, also the remaining fcc(100) clusters display a non-negligible and slowly growing proportion of stacking faults. When grown at 600 K the fcc(111) clusters are absent, but the rapid increase in the number of stacking faults (also at sizes above 200 atoms) suggests the possibility of a progressive solid-solid transition to the (111) epitaxy. Finally, when grown at 800 K, particles crystallize in both (111) and (100) epitaxies in a 4:6 proportion. No structural transition occurs during the further growth.

Several general characteristics common to the growth of the three metals are to be identified. On one hand, in all considered cases and regardless of the precise growth temperature, we find a strong overall preference for the formation of fcc(100) clusters. For both epitaxy relationships with the substrate, particles issued from growth simulations are systematically flattened and elongated if compared to their optimized counterparts—the lower the temperature, the higher the anisotropy, as illustrated in Fig. 6.

On the other hand, for the three considered metals a non-negligible proportion of fcc(111) clusters is grown at the lowest temperatures. We have encountered two kinds of scenarios. In the case of Pd and Pt, these clusters are formed by a progressive transformation of the fcc(100) ones due to a sequence of stacking faults. This mechanism is enhanced by the particularly flattened shape of particles at the lowest temperatures. The same argument supports the possibility of a slow progressive transition of the remaining Pt and Pd fcc(100) clusters toward the (111) epitaxy. At higher temperatures the particles are closer to the optimized shape and less flat. They do not transit to the (111) epitaxy. Conversely, in the case of Ag grown at lowest temperatures, the fcc(111) clusters are formed directly at the crystallization stage (less than 50 atoms). The reason is the very similar stability of the smallest (less than 50 atoms) fcc(111) and fcc(100) clusters as revealed by the $\Delta(N)$ of 0 K optimized particles in the bottom panel of Fig. 5. During the growth, these particles do not transit to the more stable (100) epitaxy. Thus, although the precise reasons are of quite a different nature, all the above fcc(111) particles grown at the lowest temperatures should be seen as due to a kinetic blocking.

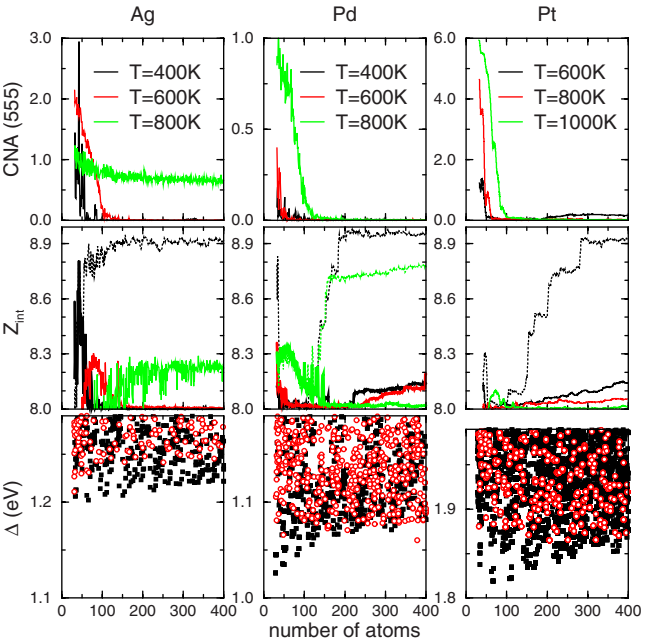

FIG. 5. (Color online) Calculated behavior of the average CNA(555) signature (top panels); of the coordination of metal atoms at the metal/oxide interface Z_{int} (middle panels): full/dashed lines for (100)/(111) epitaxy; and of specific surface energy Δ (bottom panels): full black squares for the (100) epitaxy and open red circles for the (111) one; as a function of cluster size for MgO(100)-supported Ag (left), Pd (middle), and Pt (right) clusters.

Finally, in the case of Pd, a substantial proportion of clusters in the (111) epitaxy is found in the growth at the highest considered temperature. Their direct formation at sizes only little larger than the crystallization size coincides well with a progressive inversion of the relative stability between fcc(100) and fcc(111) clusters at about 200 atoms. We note that since the remaining fcc(100) clusters preserve their epitaxial relation during the growth, they have to be considered as due to a kinetic blocking.

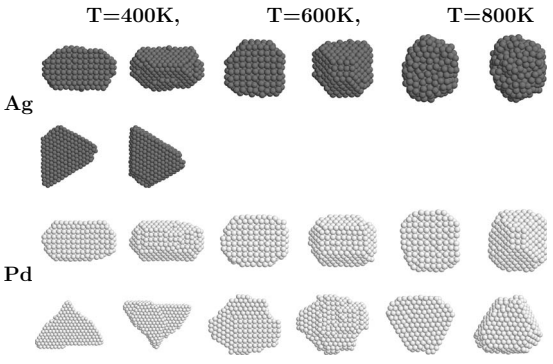

FIG. 6. Bottom view and top view snapshots of Ag and Pd clusters of 400 atoms on MgO(100) issued from growth simulations at 400, 600, and 800 K.

IV. DISCUSSION AND CONCLUSIONS

The results discussed above support the following, more general scenario of cluster atom-by-atom growth at constant temperature. Since the melting/crystallization temperature of clusters decreases rapidly at small sizes, the smallest particles are fully or partially melted. During growth, the progressive increase in particle size eventually triggers cluster crystallization. Upon crystallization, particles tend to adopt the minimal energy structure consistent with their size. For this, the results of 0 K optimization seem to give a good guideline. In most cases, since the crystallizing particles are small (50–200 atoms), they adopt the (100) epitaxy. Thus, the crystallization stage is the major factor determining the final particle shape. Indeed, in the considered temperature range, no transitions occur for clusters with shapes close to the optimized one. Only at the lowest temperatures, where the kinetic blocking is at the origin of a particularity flattened clusters, transitions to the (111) epitaxy by a sequence of stacking faults may occur.

Such a scenario is fully coherent with the experimental results obtained for Ag growth, where most of the clusters are fcc(001), and only a small fraction fcc(111).[6,38] Additionally, a somewhat flattened shape of Ag/MgO(100) clusters grown at lower temperature has been reported in GISAXS and in surface differential reflectivity spectroscopy experiments.[11]

Similarly, our present findings in the case of Pd are in good agreement with the experimental results.[8,9] We note that the predicted appearance of fcc(111) at higher temperatures does critically depend on the calculated size of fcc(100) to fcc(111) transition. As discussed in Ref. 14, the latter is very sensitive to the details of the interaction potential. Indeed, an improved Pd-Pd interaction potential does shift this transition size from 200 to about 500 atoms. Such a modification does result in an enhanced stability of fcc(100) particles in the crystallization region and impedes the crystallization of fcc(111) at higher experimental temperatures.

Finally, in the case of Pt, the present scenario suggests that, counterintuitively, the fcc(111) cluster shape, which corresponds to the 0 K equilibrium of larger Pt particles, may be unreachable even at high experimental temperatures. Indeed, at such temperatures the Pt particles crystallize in the fcc(100) epitaxy and their growth shape is close to the equilibrium (3D, not-flattened) one. As a consequence, the solid-solid transitions between fcc(100) and fcc(111) predicted at about 550 atoms for (0 K) equilibrium clusters may not occur for kinetic reasons, leaving Pt particles trapped in the fcc(100) epitaxy even at larger sizes. Conversely, kinetic trapping may be at the origin of fcc(111) clusters observed at lower temperatures in the domain of stability of the fcc(100) ones.

In summary, we have shown that since the melting/crystallization temperature decreases rapidly as a function of particle size, the smallest supported clusters are fully or partially melted at temperatures typical for the experimental growth conditions. The progressive attachment of subsequent adatoms triggers cluster crystallization at a cluster size determined principally by the temperature at which the growth takes place. Upon crystallization clusters adopt the energetically favorable form at the corresponding size. For these small sizes, the 0 K optimization seems to give a good guideline. In most considered cases it is the (100) epitaxy. This stage largely determines the final form of clusters issued for atom-by-atom growth. While solid-solid transitions at sizes beyond the crystallization size may occur, they are limited by the kinetic effects.

ACKNOWLEDGMENTS

We would like to thank R. Ferrando for stimulating discussions. We acknowledge support from the French ANR project SIMINOX Grant No. ANR-06-NANO-009-01.

[1] H. J. Freund, Surf. Sci. **500**, 271 (2002).
[2] G. Ertl and H.-J. Freund, Phys. Today **52**(1), 32 (1999).
[3] C. R. Henry, Surf. Sci. Rep. **31**, 231 (1998).
[4] H. Graoui, S. Giorgio, and C. R. Henry, Philos. Mag. B **81**, 1649 (2001).
[5] O. H. Pakarinen, C. Barth, A. S. Foster, and C. R. Henry, J. Appl. Phys. **103**, 054313 (2008); C. Barth and C. R. Henry, J. Phys. Chem. C **113**, 247 (2009).
[6] O. Robach, G. Renaud, and A. Barbier, Phys. Rev. B **60**, 5858 (1999).
[7] C. Revenant, G. Renaud, R. Lazzari, and J. Jupille, Nucl. Instrum. Methods Phys. Res. B **246**, 112 (2006).
[8] G. Renaud, R. Lazzari, C. Revenant, A. Barbier, M. Noblet, O. Ulrich, F. Leroy, J. Jupille, Y. Borensztein, C. R. Henry, J.-P. Deville, F. Scheurer, J. Mane-Mane, and O. Fruchart, Science **300**, 1416 (2003).
[9] C. Revenant, F. Leroy, R. Lazzari, G. Renaud, and C. R. Henry, Phys. Rev. B **69**, 035411 (2004).
[10] P. Nolte, A. Stierle, N. Kasper, N. Y. Jin-Phillipp, H. Reichert, A. Ruhm, J. Okasinski, H. Dosch, and S. Schoder, Phys. Rev. B **77**, 115444 (2008).
[11] R. Lazzari, G. Renaud, C. Revenant, J. Jupille, and Y. Borensztein, Phys. Rev. B **79**, 125428 (2009).
[12] J. Olander, R. Lazzari, J. Jupille, B. Mangili, J. Goniakowski, and G. Renaud, Phys. Rev. B **76**, 075409 (2007).
[13] R. Ferrando, G. Rossi, A. C. Levi, Z. Kuntova, F. Nita, A. Jelea, C. Mottet, G. Barcaro, A. Fortunelli, and J. Goniakowski, J. Chem. Phys. **130**, 174702 (2009).
[14] J. Goniakowski, A. Jelea, C. Mottet, G. Barcaro, A. Fortunelli, Z. Kuntova, F. Nita, A. C. Levi, G. Rossi, and R. Ferrando, J. Chem. Phys. **130**, 174703 (2009).
[15] A. Jelea, C. Mottet, J. Goniakowski, G. Rossi, and R. Ferrando, Phys. Rev. B **79**, 165438 (2009).
[16] W. Vervisch, C. Mottet, and J. Goniakowski, Phys. Rev. B **65**, 245411 (2002).
[17] R. P. Gupta, Phys. Rev. B **23**, 6265 (1981).
[18] V. Rosato, M. Guillopé, and B. Legrand, Philos. Mag. A **59**, 321 (1989).

[19] F. Cyrot-Lackmann and F. Ducastelle, Phys. Rev. B **4**, 2406 (1971).
[20] C. Mottet, J. Goniakowski, F. Baletto, R. Ferrando, and G. Treglia, Phase Transit. **77**, 101 (2004).
[21] F. Montalenti, F. Baletto, and R. Ferrando, Surf. Sci. **454-456**, 575 (2000).
[22] F. Baletto, R. Ferrando, A. Fortunelli, F. Montalenti, and C. Mottet, J. Chem. Phys. **116**, 3856 (2002).
[23] E. Aprà, F. Baletto, R. Ferrando, and A. Fortunelli, Phys. Rev. Lett. **93**, 065502 (2004).
[24] G. Barcaro, A. Fortunelli, G. Rossi, F. Nita, and R. Ferrando, Phys. Rev. Lett. **98**, 156101 (2007).
[25] A. Ouahab, C. Mottet, and J. Goniakowski, Phys. Rev. B **72**, 035421 (2005).
[26] G. Barcaro and A. Fortunelli, J. Chem. Theory Comput. **1**, 972 (2005).
[27] http://www.cinam.univ-mrs.fr/mottet/param/metalMgO.pdf
[28] C. Mottet and J. Goniakowski, Surf. Sci. **566-568**, 443 (2004).
[29] J. Goniakowski and C. Mottet, J. Cryst. Growth **275**, 29 (2005).
[30] H. C. Andersen, J. Chem. Phys. **72**, 2384 (1980).
[31] D. Frenkel and B. Smit, *Understanding Molecular Simulations: From Algorithms to Applications* (Academic, New York, 1996).
[32] H. F. Busnengo, W. Dong, P. Sautet, and A. Salin, Phys. Rev. Lett. **87**, 127601 (2001).
[33] D. Reinhard, B. D. Hall, D. Ugarte, and R. Monot, Phys. Rev. B **55**, 7868 (1997).
[34] F. Baletto, C. Mottet, and R. Ferrando, Phys. Rev. Lett. **84**, 5544 (2000).
[35] J. D. Honeycutt and H. C. Andersen, J. Phys. Chem. **91**, 4950 (1987).
[36] D. Faken and H. Jonsson, Comput. Mater. Sci. **2**, 279 (1994).
[37] C. L. Cleveland and U. Landman, J. Chem. Phys. **94**, 7376 (1991).
[38] C. Revenant, G. Renaud, R. Lazzari, and J. Jupille, Phys. Rev. B **79**, 235424 (2009).